PHYSICAL REVIEW E **94**, 021103(R) (2016)

# Mastering nonlinear flow dynamics for laminar flow control

Sohrab S. Sattarzadeh and Jens H. M. Fransson*
*Linné Flow Centre, KTH-Royal Institute of Technology, SE-10044 Stockholm, Sweden*
(Received 22 December 2015; published 19 August 2016)

A laminar flow control technique based on spanwise mean velocity gradients (SVGs) has recently proven successful in delaying transition in boundary layers. Here we take advantage of a well-known nonlinear effect, namely, the interaction of two oblique waves at high amplitude, to produce spanwise mean velocity variations. Against common belief we are able to fully master the first stage of this nonlinear interaction to generate steady and stable streamwise streaks, which in turn trigger the SVG method. Our experimental results show that the region of laminar flow can be extended by up to 230%.

DOI: 10.1103/PhysRevE.94.021103

For aerodynamic bodies the total drag imposed by the surrounding flow is dominated by skin-friction drag. As an example, the skin-friction drag contribution of the total drag budget of a subsonic transport aircraft amounts to more than 50% in cruise conditions [1]. Skin-friction drag results from fluid viscosity through the boundary layer (BL) formed around the body as flow passes over it. Strictly speaking, the BL flow state is either laminar or turbulent depending on its characteristics that are determined by the surface roughness, external disturbance level, and Reynolds number $\mathrm{Re}_x(= xU_\infty/\nu)$. This nondimensional number describes the ratio of inertial over viscous forces. Here $x$ is the distance relative to the point of initiation of the boundary layer, $U_\infty$ the free-stream velocity, and $\nu$ the kinematic viscosity of the fluid. Among various skin-friction drag reduction techniques laminar flow control is the most beneficial [2], since in the high $\mathrm{Re}_x$ range where both laminar and turbulent BLs can coexist, the local skin-friction coefficient is typically an order of magnitude lower in laminar compared to turbulent BLs.

In low background disturbance environments the dominating transition scenario in BLs originates from low amplitude two-dimensional disturbance waves called Tollmien-Schlichting waves (TSWs) [3–5]. These waves are the most unstable eigenmodes to the linear stability problem [6]. Among different laminar flow control techniques the spanwise mean velocity gradient (SVG) method is very promising [7–22]. The physical mechanism behind the attenuation is based on the presence of the additional spanwise turbulence production term when spanwise periodic regions of high and low speed flow, often denoted streamwise streaks, are generated. Using linear stability analysis it has been shown that this *extra* spanwise production term is locally of negative sign and can together with the viscous dissipation overcome the positive wall-normal production term, which always acts destabilizing in a BL [12]. The attenuation efficiency of TSWs by the SVG method is correlated to the amplitude of the streamwise streaks for a given spanwise wavelength, and the robustness of the streaks plays a key role in the control success, since unstable streaks at high amplitude often lead to a breakdown to turbulence. One way of producing streamwise streaks involves mounting physical control devices on the surface. These devices have evolved with respect to their performance and robustness of the generated streaks, from rectangular [9] and cylindrical [10,14] roughness elements to miniature vortex generators (MVGs) [15–18,23,24] and streamwise elongated humps [20]. Free-stream vortices have also been proven efficient to stabilize BL disturbances [22]. The drawback of fixed physical control devices is that they are always present, but there are applications where protrusive devices are not suitable or not even allowed. Hence, a new direction would be to seek solutions in setting up streamwise streaks with a minimal energy input to the control system with the feature of instantaneously being able to turn the control on and off.

The generation of streamwise streaks is a regular stage in various transition-to-turbulence scenarios. However, a prerequisite for a successful application of the SVG method is to generate streaks that are steady and stable. One of the transition scenarios involving the generation of streamwise streaks and known to lead to a *rapid* breakdown to turbulence [25], is the scenario originating from a pair of oblique waves (POW). The streaks are a result of nonlinear interaction between the oblique waves [25]. As the oblique waves decay, steady streaks are generated [26–28] and when the amplitude has grown large, the streaks become susceptible to a secondary instability and the breakdown to turbulence is inevitable. Now, if the secondary instability on the streaks can be avoided, the steady streaks may be utilized to trigger the SVG method. In the present experimental study we take advantage of the nonlinear POW excitation to generate steady and stable streaks by careful tuning of the initial forcing amplitude. Our hypothesis is that these streaks may serve as BL stabilizers via the SVG control concept and delay transition to turbulence.

The measurements were performed in a flat plate BL in the minimum-turbulence-level closed circuit wind tunnel at KTH (see Ref. [29]). A sketch of the flat plate mounted horizontally in the wind tunnel test section is shown in Fig. 1 where the coordinate system $(x,y,z)$ is introduced. The streamwise velocity component is denoted by $U$ with the small letter $u$ corresponding to the disturbance velocity. The external pressure gradient along the plate was nullified by adjusting the ceiling in the test section to obtain an ideal zero-pressure-gradient BL for a free-stream velocity of $U_\infty = 6\,\mathrm{m\,s^{-1}}$, which was kept constant for all the measurements.

Boundary layer disturbances were artificially introduced by means of blowing and suction through two spanwise-oriented disturbance slots located at $x_{1\mathrm{st}}^{\mathrm{dist.}} = 160$ mm and $x_{2\mathrm{nd}}^{\mathrm{dist.}} =$

*Author to whom correspondence should be addressed: jensf@kth.se

 

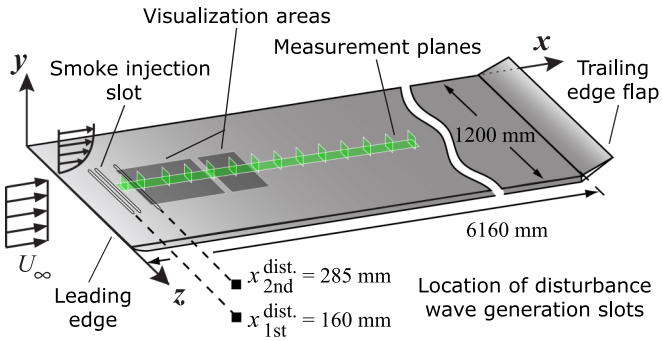


FIG. 1. Schematic of the flat plate in the wind tunnel test section. The measurement planes consist of a horizontal and a series of cross-sectional planes. Smoke injection slot is located at $x = 180$ mm. Locations of disturbance wave generation slots are depicted in the figure.

285 mm. The slots of 270 mm × 0.8 mm opening were made in a plug, which is flash-mounted in the plate in order to avoid any unintentional disturbances (see Ref. [30] where a similar slot was used). Two measurement configurations C1 and C2 were investigated consisting of POW excitation at the upstream and the downstream disturbance slot as the control, respectively, and where TSWs were consequently excited through the other slot. Note that in some measurement cases the TSW excitation was turned off in order to investigate the characteristics of the streaky BL generated by POW. With respect to the disturbance type the slots were connected via two sets of 36 tubes to either a single (TSW) or a set of six (POW) loudspeakers driven by sinusoidal voltage signals controlled by a computer. The single loudspeaker, driven by the voltage signal $E_{TSW} \propto \sin(\omega_1 t)$, renders uniform sinusoidal waves in the spanwise direction where $\omega_1 (= 2\pi f_0)$ is the fundamental angular frequency and $f_0$ the frequency of the generated disturbance waves. On the other hand, the set of six loudspeakers, driven by the voltage signal $E_{POW} \propto \sin(\omega_1 t)\cos(n\pi/3)$, where $n$ is the number of the loudspeaker 1–6, render a disturbance corresponding to the superposition of two oblique waves with opposite spanwise propagation directions. Here the tubes are connected sequentially to the loudspeakers in an order that loudspeaker $n$ is connected to tube $6(j-1)+n$ where $j = 1$–6. The POW spanwise wavelength is hence set to $\lambda_z^{POW} = 44$ mm that corresponds to the spanwise width of six tubes. The generated POW have the initial amplitude distribution $A_{initial}^{POW}(t,z) = A_0^{POW}\sin(\omega_1 t)\cos(\beta_1 z)$, where $A_0^{POW}$ is the forcing amplitude and $\beta_1 (= 2\pi/\lambda_z^{POW})$ is the fundamental POW spanwise wave number. For the excited disturbances we use the nondimensional frequency $F = 2\pi f_0 \nu/U_\infty^2 \times 10^6$ throughout this Rapid Communication.

Phase triggered single-probe hot-wire anemometry measurements with temporal and spatial resolutions of 5 kHz and 0.6 mm, respectively, were carried out in cross-sectional $yz$ planes in the BL as well as a horizontal $xz$ plane above the flat plate. The horizontal plane was located at $y = 1.72\delta(x)$ in the wall-normal direction, where $\delta\ (=\sqrt{x\nu/U_\infty})$ is the BL scale. The phase triggering allows the disturbance field to be accurately reconstructed in the linear regime from single-point measurements. The smoke flow visualizations were recorded by three synchronized CCD cameras (1280 × 1024 pixels each) positioned in series in the streamwise direction. The smoke sheet was injected through a spanwise-oriented slot of 270 mm × 0.8 mm openning in the flat plate at $x = 180$ mm.

The velocity field can be transformed to spatiotemporal Fourier modes with the notation $(\omega,\beta)$, normalized by $\omega_1$ and $\beta_1$. A graph of the dominating modes excited in oblique transition is shown in Fig. 2(a), where only modes with positive $\beta$ are depicted due to symmetry in the spanwise direction. The $(1, \pm 1)$ modes correspond to POW and the initial flow consists of a standing wave pattern. The POW excite counter-rotating streamwise vortices with $(0, \pm 2)$ modes through quadratic nonlinearity [25], which consequently generate the streamwise streaks with similar Fourier components through the lift-up effect [31]. The spanwise wavelength of the streaks is therefore $\lambda_z^{ST} = \lambda_z^{POW}/2$. The experimentally measured POW and generated streamwise streaks are shown in Figs. 2(c) and (d), respectively, as unsteady $u_u = U(x,z,t^*) - U^t(x,z)$ and steady $u_s = U^t(x,z) - U(x)^{tz}$ disturbances. Superscripts $t$ and/or $z$ denote averaged dimensions and $t^*$ a particular time. The forced periodic disturbances are shown as the unsteady disturbances, i.e., $u_u$, at the given time $t^*$, in Fig. 2(c). As the POW disturbances propagate downstream $\Lambda$ vortices are developed in a staggered pattern similar to the $N$-type breakdown scenario [26]. The generated streaks are exhibited as steady disturbances, i.e., $u_s$, with their high-speed regions located at the nodal points of the standing-wave pattern.

The amplitudes of the TSW and the POW disturbances are obtained as an integral measure over cross-sectional $yz$ planes

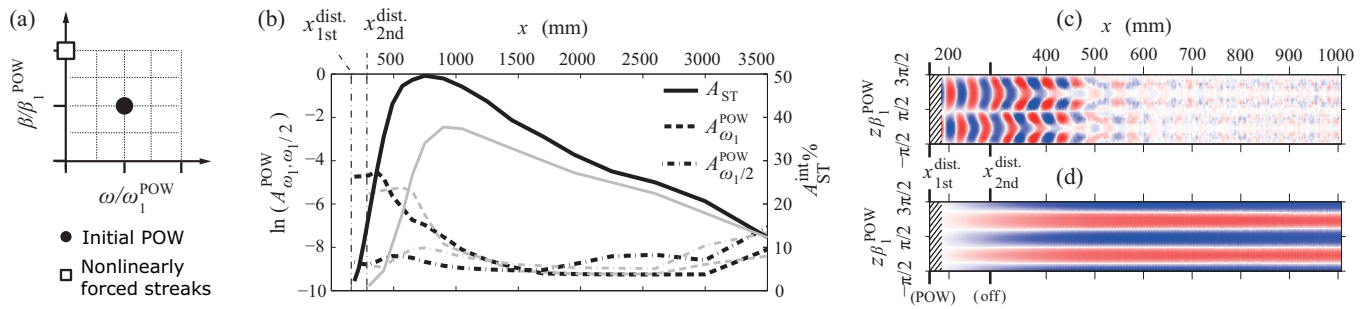


FIG. 2. (a) Graph of the dominating modes excited in oblique transition. (b) Amplitude of POW ($A_{\omega_1}^{POW}$), its subharmonic ($A_{\omega_1/2}^{POW}$) and the generated streamwise streaks ($A_{ST}$) for C1 (black) and C2 (gray) configurations. $F_{POW} = 130$. (c) and (d) Reconstructed unsteady $u_u$ (instantaneous) and steady $u_s$ disturbances, respectively, for C1 configuration and $F_{POW} = 130$. In (d) high-speed streaks are located at $z\beta_1^{POW} = -\pi/2$, $\pi/2$, and $3\pi/2$.

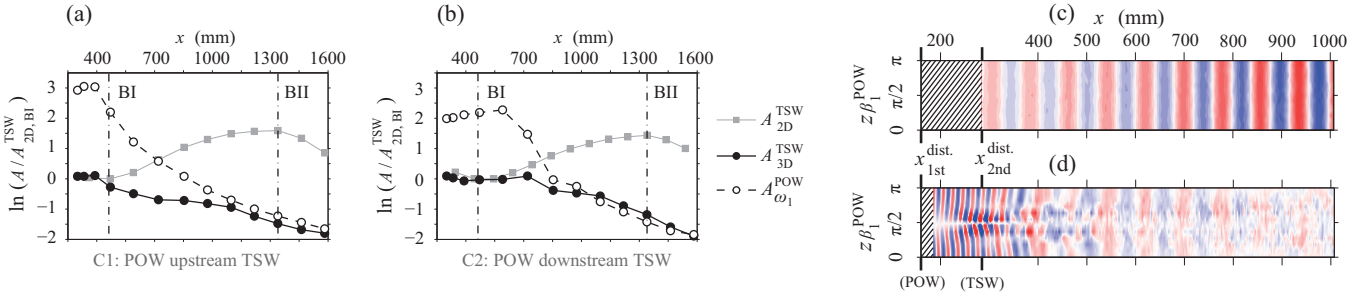


FIG. 3. (a) and (b) Disturbance amplitude growth curves for uncontrolled TSW ($A_{2D}^{TSW}$), controlled TSW ($A_{3D}^{TSW}$), and POW ($A_{\omega_1}^{POW}$) for C1 (a) and C2 (b) configurations. $F_{TSW} = 100$ and $F_{POW} = 130$. (c) and (d) Reconstructed instantaneous unsteady disturbances $u_u$ for uncontrolled (c) and controlled (d) cases. $F_{TSW} = 130$ and $F_{POW} = 340$.

based on the local disturbance amplitude as

$$A^{\text{dist.}}(x) = \int_0^{\pi} \int_0^{\eta^*} \frac{A^{\text{dist.}}_{\text{local}}(x,\eta,\zeta)}{U_\infty} d\eta\, d\zeta, \qquad (1)$$

where $\zeta = z\beta_1^{POW}$ and $\eta = y/\delta$ with $\eta^* = 9$. Depending on the disturbance type the superscript (dist.) is replaced by TSW or POW. For the POW disturbance the amplitude of both fundamental ($A_{\omega_1}^{POW}$) and subharmonic ($A_{\omega_1/2}^{POW}$) temporal modes are investigated. Similarly, an integral measure is defined for the streak amplitude as (see Ref. [16])

$$A_{ST}(x) = \int_0^{\pi} \int_0^{\eta^*} \frac{|U(x,\eta,\zeta) - U^z(x,\eta)|}{U_\infty} d\eta\, d\zeta. \qquad (2)$$

For both amplitude measures the spanwise integration is over $\lambda_z^{POW}/2 (= \lambda_z^{ST})$ as the flow is symmetric in the spanwise direction. As shown in Fig. 2(b), for both C1 and C2 configurations, $A_{\omega_1}^{POW}$ decays, meanwhile $A_{ST}$ grows to a maximum streak amplitude $A_{ST}^{max}$. After $A_{ST}^{max}$ the streak amplitude decays exponentially as a consequence of viscous dissipation. The growth of the subharmonic mode ($A_{\omega_1/2}^{POW}$), which imposes the secondary instability on the streaks [26], is here inhibited by tuning $A_0^{POW}$ except for a small region at the end of the streamwise domain, and hence the streaks remain stable.

The TSW growth curves in the linear regime (i.e., with low initial forcing amplitude) are shown in Figs. 3(a) and 3(b) for C1 and C2 configurations, respectively, where uncontrolled ($A_{2D}^{TSW}$) and controlled ($A_{3D}^{TSW}$) cases are plotted together with the evolution of $A_{\omega_1}^{POW}$. Here amplitudes are normalized with the uncontrolled TSW amplitude at branch I (BI) of the neutral stability curve. An initial TSW-POW interaction region is observed in the disturbance field whereafter $A_{3D}^{TSW}$ is attenuated compared to $A_{2D}^{TSW}$. The interaction region is based on the location where $A_{\omega_1}^{POW}$ starts to decay. The attenuation of TSW in the horizontal $xz$ plane is shown in Figs. 3(c) and 3(d) where $u_u$ is plotted for uncontrolled (c) and controlled (d) cases.

To pursue the main goal of transition to turbulence delay the control has to be tested on nonlinear TSWs, i.e., with high initial forcing amplitudes. This was done for a range of individually forced $F_{TSW}$ in both C1 and C2 configurations. The results are plotted in the top and bottom rows of Fig. 4, respectively, as the disturbance energy evolution in the $F$-$\text{Re}_x$ plane for both uncontrolled and controlled cases. Figures 4(a) and 4(e) show the disturbance energy $(u_{rms}/U_\infty)^2$ evolution for the uncontrolled reference BL for C1 and C2, respectively, where nonlinear TSWs force the BL to breakdown to turbulence. The transition locations corresponding to the intermittency value of $\gamma = 0.5$ are plotted

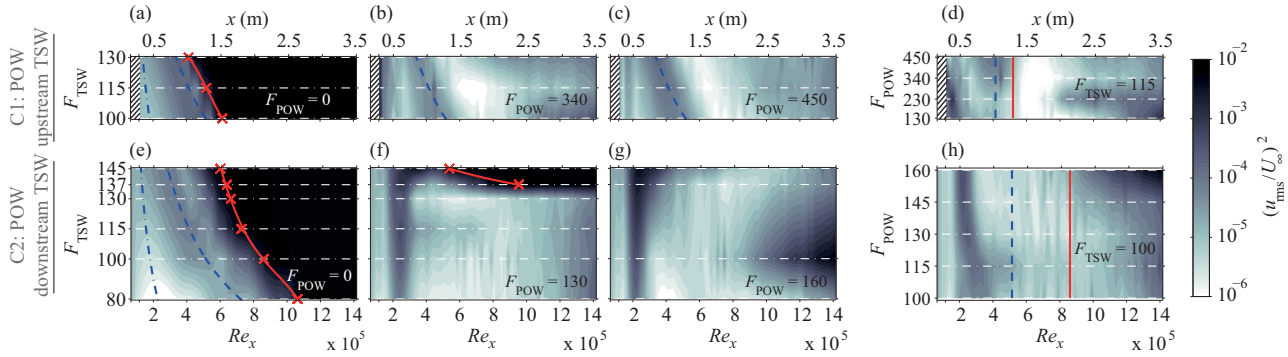


FIG. 4. Disturbance energy evolution in the $F$-$\text{Re}_x$ plane (measured at $y/\delta = 0.86$ and $z\beta_1^{POW} = 0$). Measured frequencies, to produce the contour plots, are indicated by white dashed-dotted lines and tick marks on the vertical axes. Branches I and II of the neutral stability curve for the reference BL are plotted as dark dashed-dotted and dashed lines, respectively. Transition locations ($\gamma = 0.5$) are plotted as cross symbols. Top row: C1 configuration; (a), (b), and (c) correspond to $F_{POW} = 0$ (uncontrolled reference BL), $F_{POW} = 340$, and $F_{POW} = 450$, respectively. (d) Varying $F_{POW}$ for fixed $F_{TSW} = 115$. Bottom row: C2 configuration; (e), (f), and (g) correspond to $F_{POW} = 0$, $F_{POW} = 130$, and $F_{POW} = 160$, respectively. (h) Varying $F_{POW}$ for fixed $F_{TSW} = 100$. Vertical solid lines indicate transition locations for uncontrolled cases in (d) and (h).

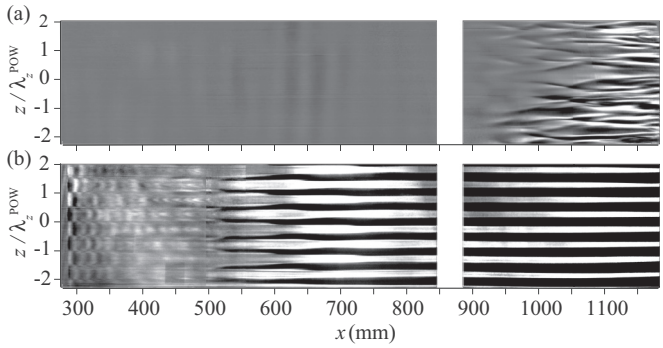


FIG. 5. Smoke flow visualization for C2 with $F_{TSW} = 145$ and $F_{POW} = 160$. (a) Control off and (b) control on.

as cross symbols. The intermittency is a statistical measure of the proportion of laminar versus turbulent flow sweeping the hot-wire probe. Branches I and II of the neutral stability curve for the reference BL are also plotted as dashed-dotted and dashed lines, respectively. For C1 the controlled cases with $F_{POW} = 340$ and $F_{POW} = 450$ are plotted in Figs. 4(b) and 4(c) where an attenuated branch II is observed at the same location compared to the uncontrolled case whereafter the disturbances decay. The successful extension of laminar flow depends on $F_{TSW}$ and Figs. 4(a)–4(c) show that this extension is 125%–230% in the range $F_{TSW} = 100$–130.

The effect of $F_{POW}$ for a fixed $F_{TSW} = 115$ is shown in Fig. 4(d) where branch II and the transition location of the uncontrolled case are plotted as dashed and solid lines, respectively. Here the main conclusion is that there is an initial TSW-POW interaction region with high disturbance energy. This region diminishes with increasing $F_{POW}$ since the POWs then decay further upstream. The initial TSW-POW interaction is inevitable for C2 as POWs are excited in the presence of the TSW. For this configuration, the controlled cases with $F_{POW} = 130$ and 160 are shown in Figs. 4(f) and 4(g) where branch II is inhibited for all $F_{TSW}$. Noteworthy is that the streamwise location of the onset of the initial interaction region is fixed and independent of $F_{POW}$, but as $F_{POW}$ is increased the extent of the initial interaction region becomes smaller [see Fig. 4(h)].

Smoke flow visualizations with control off and control on are shown in Figs. 5(a) and 5(b), respectively. In Fig. 5(b) the initial TSW-POW interaction is illustrated as a secondary instability of varicose type on the streaks at the initial stage of their formation [see the range 550–750 mm in Fig. 5(b)]. The frequency of the varicose mode corresponds to the TSW frequency $F_{TSW}$ and is damped further downstream for the case shown in Fig. 5 since the streaks become stable. However for $F_{POW} < F_{TSW}$ the high amplitude of the varicose instability mode leads to transition to turbulence [see $F_{TSW} = 145$ in Fig. 4(f)] and hence to a failure of the control method. This is believed to be associated with the disruptive role of high amplitude TSWs on the generation of streaks in the superimposed disturbance field for cases with $F_{POW} < F_{TSW}$ where $\lambda_x^{POW} > \lambda_x^{TSW}$. However, for $F_{POW} > F_{TSW}$ the transition to turbulence is successfully delayed and therefore we introduce it as the control condition. The control was also tested successfully for high amplitude white noise disturbances.

In the present experimental study we show that nonlinear POWs can be used successfully as a base flow modulator for the SVG laminar flow control method as long as $F_{POW} > F_{TSW}$. This eliminates the demand of constant presence of physical devices such as roughness elements, MVGs, or surface patterns for base flow modulations and allows the control to be turned on and off. We show that the nonlinear dynamics in the rapid oblique breakdown scenario can be tuned in order to generate highly modulated stable streaks where their amplitude and streamwise extent are solely controlled by POW forcing frequency and initial forcing amplitude. As a result we present a significant transition-to-turbulence delay, leading to an extension of laminar flow by up to 230%, for highly nonlinear TSWs in the BL. The control strategy is proven to work for a wide frequency range and different configurations by applying the control upstream of as well as downstream from the TSW excitation location.

J.H.M.F. acknowledges the European Research Council for its financial support of the AFRODITE project ERC-StG-2010-258339.

[1] R. D. Joslin, Annu. Rev. Fluid Mech. **30**, 1 (1998).
[2] J. E. Green, AIAA paper No. 2008-3738 (2008).
[3] W. Tollmien, Nachr. Ges. Wiss. Göttingen 21-24 (1929) [National Advisory Committee for Aeronautics Report No. TM 609, Washington, DC, 1931].
[4] H. Schlichting, Z. Angew. Math. Mech. **13**, 260 (1933).
[5] G. B. Schubauer and H. K. Skramstad, J. Aero. Sci. **14**, 69 (1947).
[6] H. B. Squire, Proc. R. Soc. London, Ser. A **142**, 621 (1933).
[7] Y. S. Kachanov and O. I. Tararykin, Izv. Sib. Otd. Akad. Nauk SSSR, Ser. Tech. Nauk **18**, 9 (1987).
[8] K. J. A. Westin, A. V. Boiko, B. G. B. Klingmann, V. V. Kozlov, and P. H. Alfredsson, J. Fluid Mech. **281**, 193 (1994).
[9] A. A. Bakchinov, G. R. Grek, B. G. B. Klingmann, and V. V. Kozlov, Phys. Fluids **7**, 820 (1995).
[10] J. H. M. Fransson, L. Brandt, A. Talamelli, and C. Cossu, Phys. Fluids **17**, 054110 (2005).
[11] S. S. Sattarzadeh and J. H. M. Fransson, Exp. Fluids **56**, 1 (2015).
[12] C. Cossu and L. Brandt, Eur. J. Mech.: B Fluids **23**, 815 (2004).
[13] L. Siconolfi, S. Camarri, and J. H. M. Fransson, J. Fluid Mech. **784**, 596 (2015).
[14] J. H. M. Fransson, A. Talamelli, L. Brandt, and C. Cossu, Phys. Rev. Lett. **96**, 064501 (2006).
[15] S. Shahinfar, S. S. Sattarzadeh, J. H. M. Fransson, and A. Talamelli, Phys. Rev. Lett. **109**, 074501 (2012).
[16] S. Shahinfar, J. H. M. Fransson, S. S. Sattarzadeh, and A. Talamelli, J. Fluid Mech. **733**, 1 (2013).

[17] S. Shahinfar, S. S. Sattarzadeh, and J. H. M. Fransson, J. Fluid Mech. **749**, 1 (2014).
[18] S. S. Sattarzadeh, J. H. M. Fransson, A. Talamelli, and B. E. G. Fallenius, Phys. Rev. E **89**, 061001(R) (2014).
[19] S. S. Sattarzadeh and J. H. M. Fransson, Phys. Fluids **26**, 124103 (2014).
[20] R. S. Downs and J. H. M. Fransson, J. Fluid Mech. **754**, 39 (2014).
[21] P. Schlatter, E. Deusebio, R. de Lange, and L. Brandt, Int. J. Flow Contr. **2**, 259 (2010).
[22] L. Siconolfi, S. Camarri, and J. H. M. Fransson, J. Fluid Mech. **764**, R2 (2015).
[23] J. H. M. Fransson, B. E. G. Fallenius, S. Shahinfar, S. S. Sattarzadeh, and A. Talamelli, J. Phys.: Conf. Ser. **318**, 032007 (2011).
[24] J. H. M. Fransson and A. Talamelli, J. Fluid Mech. **698**, 211 (2012).
[25] P. J. Schmid and D. S. Henningson, Phys. Fluids A **4**, 1986 (1992).
[26] Y. S. Kachanov, Annu. Rev. Fluid Mech. **26**, 411 (1994).
[27] S. Berlin, M. Wiegel, and D. S. Henningson, J. Fluid Mech. **393**, 23 (1999).
[28] P. A. Elofsson and P. H. Alfredsson, Eur. J. Mech. B-Fluids **19**, 615 (2000).
[29] B. Lindgren and A. V. Johansson, KTH Mechanics Technical Report No. KTH/MEK/TR02/13SE, 2002, http://www.mech.kth.se/∼jensf/Lindgren2002.
[30] V. Gaponenko and Y. Kachanov, in Proceedings of ICMAR, Part 1, 1994 (unpublished), pp. 125.
[31] M. T. Landahl, J. Fluid Mech. **98**, 243 (1980).